Implementation of a Leader-Follower Controller for a Skid-Steering Wheel-Legged Robot

Luc Xuan Tu Phung, Inna Sharf
Department of Mechanical Engineering
McGill University
Montreal, Canada
luc.phung@mail.mcgill.ca, inna.sharf@mcill.ca

Blake Beckman
Autonomous Systems Operations – Ground Group
Defence Research and Development Canada
Medicine Hat, Canada
Blake.Beckman@drdc-rddc.gc.ca

***Abstract*—In this paper, we present a leader-follower controller for the Micro-Hydraulic Toolkit (MHT), a skid-steering wheel-legged robot designed by Defence Research and Development Canada – Suffield Research Centre. The objective of the controller is to maneuver the MHT towards a desired position with respect to a designated leader. Using the range and bearing of the leader from the robot, the leader-follower controller computes the desired wheel velocities of the MHT to achieve leader-follower formation control. In addition to performing wheeled locomotion to follow the leader, the MHT is capable of using its legs to reconfigure its posture. Thus, moving beyond standard implementations, the leader-follower control strategy presented in this paper is combined with a velocity-based inverse kinematics controller developed in previous work to control the posture of the MHT during leader-follower maneuvers. The results of the leader-follower scenarios implemented in simulation and on the physical MHT demonstrate the robot's ability to execute leader-follower formation control and posture control simultaneously, adding to the versatility of the vehicle to negotiate uneven terrains.**

Keywords—leader-follower controller; skid-steering robot; wheel-legged robot; posture control; vision system

I. INTRODUCTION

In recent years, researchers in the robotics community have demonstrated a growing interest in the implementation of follower behaviors on mobile robots. The follower behaviors can be applied to coordinate groups of unmanned vehicles to perform complex tasks, such as exploration of a new environment [1], or to assist a human user in applications such as a load bearing mule [2].

This paper investigates the leader-follower control problem in the context of a wheel-legged robot following a leader. Existing literature on leader-follower control is mainly presented in the framework of formation control of multi-robot systems. The challenge consists of maneuvering members of a team of mobile robots to maintain a desired formation as the system moves as a whole. While different solutions have been proposed to coordinate teams of mobile robots, the leader-follower approach is predominantly used to achieve formation control of multi-robot systems due to its simplicity, flexibility and low computational cost [3].

In the leader-follower approach, a member of the multi-robot system, defined as the leader, moves along the desired trajectory of the formation. The other robots, defined as followers, are required to maintain their desired relative positions with respect to the leader. Different solutions have been proposed in literature to implement leader-follower behaviors on mobile robots. Ghommam et al. [4] developed a controller that uses the configuration of the leader to determine the desired configuration and velocities of the follower to maintain the formation. Then, the controller executes a trajectory tracking algorithm to maneuver the follower to its desired state and achieve leader-follower formation control. Consolini et al. [5] proposed a leader-follower control strategy to direct nonholonomic robots with input constraints towards a desired range and bearing from a lead vehicle. Their controller uses the configuration and linear velocity of the leader to calculate the desired velocities of the followers to achieve formation control. Choi and Choi's [6] leader-follower controller is designed to guide a follower robot towards its desired position with respect to a leader using the linear velocity of the leader and the positioning error of the follower. Each of the aforementioned, albeit different, strategies allows mobile robots to achieve leader-follower formation control. However, they require knowledge of the full configuration and velocities of the leader. In real systems, such as the platform detailed in this work, practical sensors may not provide sufficiently accurate measurements to satisfy this condition.

In this work, we present a leader-follower control strategy for the Micro-Hydraulic Toolkit, a skid-steering wheel-legged robot designed by Defence Research and Development Canada – Suffield Research Centre (Fig. 1). The design of the MHT allows the robot to combine the energy efficiency of wheeled vehicles and the ability to adapt to uneven terrains of legged locomotion. The motion planning and control of wheel-legged systems have been explored by several other researchers, notably by Iagnemma and Dubowsky [7] in the context of planetary exploration. In [7], the motion planning methodology and reconfiguration of the vehicle are demonstrated with the JPL Sample Return Rover (SRR), but the terrain traversal is carried out as a sequence of short distance travel, stopping and posture adjustment cycles.

DRDC-RDDC-2016-P018

In previous work, Thomson et al. [8] implemented a velocity-based inverse kinematics controller that allows the MHT to reconfigure its posture. This controller was developed based on the control algorithm of Hylos [9] due to the similarities of its design with the MHT. However, unlike Hylos and SRR, the MHT is not equipped with a steering mechanism for its wheels. Therefore, a separate leader-follower control algorithm was developed for the MHT: it uses the range and bearing of the leader to compute the desired wheel velocities to maneuver the robot towards the leader. The leader-follower controller is implemented in *parallel* with the inverse kinematics controller of the MHT, allowing the robot to execute leader-follower behaviors and posture control *simultaneously*. This increases the vehicle's versatility to follow a designated human leader or another vehicle on uneven terrains.

In the following section, the kinematic model of the MHT and the leader-follower formation framework are detailed. Section III describes the final control architecture of the MHT and the leader-follower controller formulation for the robot. In Section IV, we present the results of two leader-follower maneuvers implemented in simulation and on the physical platform of the MHT. Finally, Section V summarizes the work of this paper.

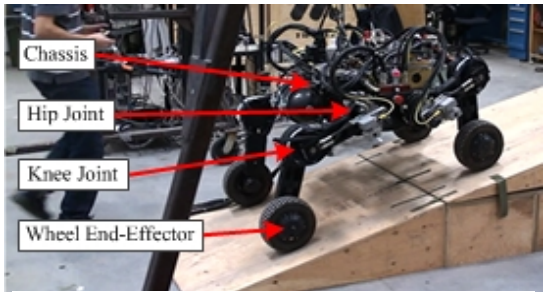

Figure 1: Micro-Hydraulic Toolkit

II. Relevent Kinematics

This section addresses the kinematic model of the MHT and the leader-follower formation framework applied in the development of the leader-follower controller.

A. Kinematic Model of the MHT

The MHT is composed of a chassis and four leg assemblies. Each leg has a hip joint, a knee joint and a wheel end-effector, which allows the robot to reconfigure its posture while navigating uneven terrains (Fig. 1). The design of the MHT is further detailed in [10].

Being a skid-steering vehicle, the MHT can only execute turning maneuvers by driving its left and right wheels at different angular velocities. This leads to the skidding of the wheels, which is not possible to accurately capture in the kinematic model of the robot. In the design of the leader-follower controller, we assumed that the skidding resistance of the wheels is negligible. Therefore, the kinematics of the MHT can be sufficiently represented by the kinematic model of a two-wheel differentially driven vehicle, in particular:

$$v_x = (r_w/2)(\omega_r + \omega_l) \quad (1)$$

$$\omega = (r_w/2c)(\omega_r - \omega_l) \quad (2)$$

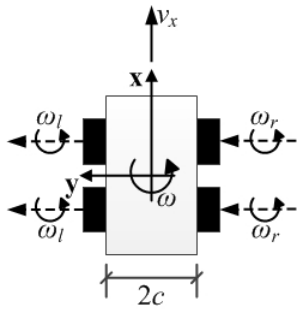

Figure 2: Micro-Hydraulic Toolkit Kinematic Model

where v_x is the linear velocity of the robot, ω is its turning rate, ω_r and ω_l are the angular velocities of the right and left wheels respectively, r_w is the wheels' radius and c is half the distance separating the left and right wheels (Fig. 2).

B. Leader-Follower Formation Framework

In consideration of the exteroceptive sensors used by the MHT to track the leader, it was assumed that only the range and bearing of the leader with respect to the robot are available to the leader-follower controller. Based on this assumption, we developed a leader-follower formation framework building on the work of Choi and Choi [6]. The leader-follower formation is defined by a desired range (r_d) and a desired bearing (γ_d) of the leader specified in the follower's reference frame. Let the configuration of the leader and of the follower be defined by:

$$\mathbf{R} = [\, X \;\; Y \;\; \theta \,]^{\mathrm{T}} = [\, \mathbf{P}^{\mathbf{T}} \;\; \theta \,]^{\mathrm{T}} \quad (3)$$

where X and Y characterize the leader or the follower's position, and θ describes its orientation.

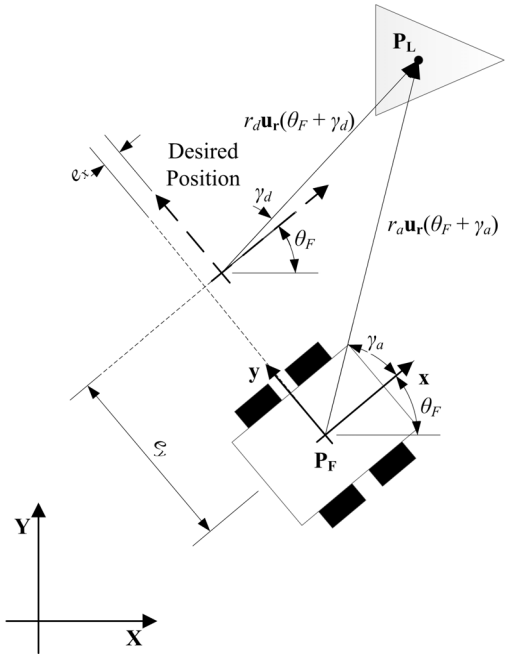

Figure 3: Leader-Follower Formation Framework

The follower is said to have achieved the desired leader-follower formation when (4) is satisfied, i.e.:

$$\mathbf{P_F} = \mathbf{P_L} - r_d\,\mathbf{u_r}(\theta_F + \gamma_d) \tag{4}$$

where $\mathbf{P_F}$ and $\mathbf{P_L}$ are the positions of the follower and of the leader respectively, and $\mathbf{u_r}(\theta_F + \gamma_d)$ is a unit vector with orientation $(\theta_F + \gamma_d)$, i.e. from the follower`s desired position to the leader (Fig. 3).

III. MHT Controller

In this section, the architecture of the MHT's controller is summarized and the leader-follower controller is presented. The final controller implemented on the MHT for this work is a velocity based decoupled posture and leader-follower controller (Fig. 4).

The posture controller of the MHT was designed based on the control algorithm of Hylos [9]. The controller's inputs are the desired posture of the robot ($\mathbf{p_d}$) and its actual posture ($\mathbf{p_a}$). The posture of the MHT is defined by the chassis pitch and roll angles, the chassis height and the wheels' positions. Using the inverse kinematic model of the MHT, the posture controller computes the desired angular rates of the hip joints, knee joints and wheel end-effectors of the robot to achieve and maintain the desired posture. The performance of the controller was verified in simulation by Thomson et al. [8] and on the physical MHT by Wong [11]. The posture controller of the MHT is further detailed in [11].

The objective of the leader-follower controller is to compute the desired wheels angular velocities of the MHT to achieve leader-follower formation control. First, the control algorithm calculates the positioning errors of the robot with respect to its desired position. Using the actual range (r_a) and bearing (γ_a) of the leader from the MHT, the controller determines the positioning errors of the vehicle with the following equations from [6]:

$$e_x = r_a\cos(\gamma_a) - r_d\cos(\gamma_d) \tag{5}$$

$$e_y = r_a\sin(\gamma_a) - r_d\sin(\gamma_d) \tag{6}$$

where e_x is the longitudinal positioning error of the MHT and e_y is its lateral positioning error (Fig. 3).

Next, the leader-follower controller determines the desired linear velocity (v_{xd}) and turning rate (ω_d) of the MHT to achieve the desired range and bearing from the leader. The desired linear velocity is computed using the longitudinal positioning error of the robot with a PID control law. The desired turning rate of the vehicle is calculated with the lateral positioning error of the MHT and a PD control law combined with a modified integral term from [12] to counteract the skidding resistance of the wheels. Note that differently from [6], our controller does not employ the leader's velocity to compute the desired velocities of the follower. The desired velocities of the robot are thus defined as:

$$v_{xd} = K_{Px}\,e_x + K_{Ix}\int e_x\,dt + K_{Dx}\,(de_x/dt) \tag{7}$$

$$\omega_d = K_{Py}\,e_y + K_{Iy}\,\mathrm{sign}(e_y)\int e_y\,\mathrm{sign}(e_y)dt + K_{Dy}\,(de_y/dt) \tag{8}$$

where K_{Px}, K_{Ix}, K_{Dx}, K_{Py}, K_{Iy} and K_{Dy} are the gains of the leader-follower controller.

In the last stage of the leader-follower controller, the desired rates of the left (ω_{ld}) and right (ω_{rd}) wheels are calculated using the results of (7) and (8). The controller determines the desired wheel velocities using (1) and (2) as follow:

$$\omega_{ld} = (v_{xd} - c\omega_d) / r_w \tag{9}$$

$$\omega_{rd} = (v_{xd} + c\omega_d) / r_w \tag{10}$$

The outputs of the leader-follower controller are subsequently combined with the desired angular rates of the wheels computed by the posture controller. The final results of the combined two controllers are the desired angular rates of the hip joints, knee joints and wheels of the robot (assembled in $\dot{\mathbf{q}}_\mathbf{d}$). Lastly, a PID control law is applied to the joint rate errors to obtain the voltage commands to the joints of the MHT (combined in $\mathbf{V}$) for the robot to achieve leader-follower formation control and posture control simultaneously.

IV. Results

To assess the performance of the leader-follower controller presented in this paper, we implemented different leader-follower maneuvers in simulation and on the physical MHT robot. The maneuvers detailed in this work were first implemented in simulation using a high-fidelity model of the MHT in LMS Virtual.Lab Motion developed by LMS engineers. The model incorporates various dynamic properties of the robot such as its mass distribution and the wheel-ground contact forces [13]. The controller of the MHT resides in Matlab/Simulink; therefore, co-simulations were performed using Matlab/Simulink and LMS Virtual.Lab Motion.

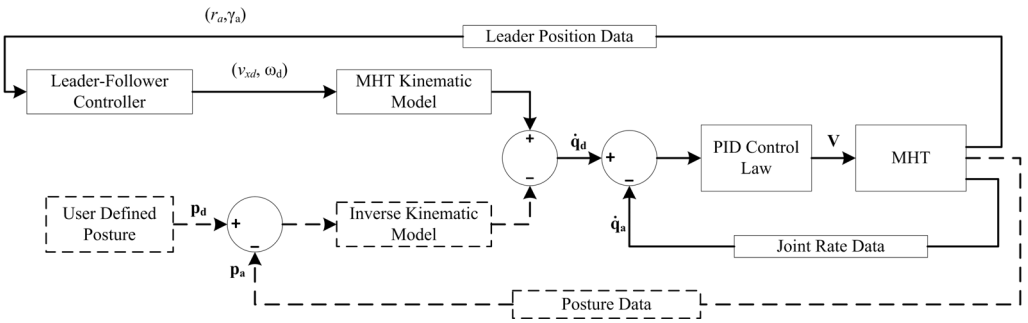

Figure 4: MHT Controller Architecture

The ultimate validation of the leader-follower controller was achieved with the physical MHT robot. The experiments were performed in a laboratory environment at the facilities of Defence Research and Development Canada – Suffield Research Centre. In the experiments, the leader is defined as a ball of uniform color and is moved along a pre-defined trajectory by a human user. The range and bearing of the leader are measured using a vision system installed on the MHT (detailed in the following subsection). To prevent the leader-follower controller and the robot from reacting to small oscillations in the range and bearing measurements, we added dead-zones in the positioning errors computation stage of the controller on the physical MHT. The controller is uploaded to the robot from Matlab/Simulink using Freescale's Codewarrior program. The gains of the leader-follower controller in (7) and (8) were calibrated for the physical robot. The same gains were used in the simulations.

A. Vision System of the MHT

To track the leader, the MHT uses a vision system composed of an IEEE 1394 Flea camera from Point Grey Research mounted on a Pan-Tilt Unit-D46-17.5 from FLIR System Inc. (Fig. 5).

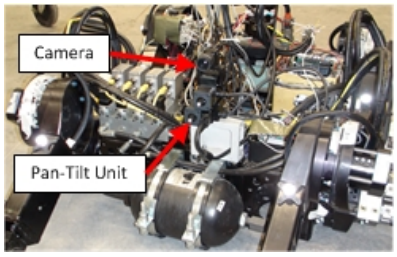

Figure 5: MHT Vision System

Since the tests with the MHT were performed in a controlled environment, we used a ball of uniform color as the designated leader to simplify the tracking algorithm implemented on the vision system. First, the vision system uses the Continuous Adaptive Meanshift (CamShift) algorithm [14] to detect the leader in the images from the camera. Then, a combination of color-based tracking algorithm and contour detection algorithm is executed to measure the radius and position of the ball in the images. To maintain the leader in the field of view of the camera, the pan-tilt unit uses the perceived position of the ball in the images to rotate the camera towards the leader. The bearing of the leader is computed using the horizontal position of the ball in the field of view of the camera and the pan angle feedback from the pan-tilt unit. To calculate the range of the leader, we apply a function that correlates the perceived radius of the ball in the images and its distance from the MHT. This function was generated from a separate set of calibration experiments. The vision algorithm was implemented on the vision system of the MHT using the Robotic Operating System (ROS) and the OpenCV library [15].

B. Leader-Follower Maneuver on Flat Terrain

To test the leader-follower controller, we first implemented multiple leader-follower maneuvers in simulation and with the physical MHT prototype in which the robot travels on a flat surface. In these tests, the leader moves along linear, quarter-circular, corner and perpendicular trajectories. The MHT was then required to follow the leader to achieve the desired range and bearing from the leader. In this paper, we present a maneuver in which the leader moves along a quarter-circular trajectory of 3 m radius. The MHT must achieve a range and bearing of 1 m and 0º, respectively, from the leader. During the test, the posture controller is applied to maintain the MHT at a constant steering posture characterized by a zero chassis pitch and roll angles, a chassis height of 0.409 m and a wheel separation of 0.450 m (Fig. 6). This particular posture was selected since it allows the robot to turn in both simulation and experiments while maintaining a good stability margin [11].

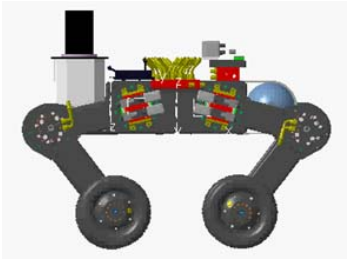

Figure 6: MHT Steering Posture

Experiments under open-loop control of the wheels revealed that the maximum linear velocity and turning rate of the MHT in the steering posture are 1.4 m/s and 22º/s in simulation, and 0.44 m/s and 18º/s with the physical robot [11]. We observe that while the maximum linear velocities of the MHT in simulation and experiment are significantly dissimilar, the difference between the maximum turning rates is marginal. This indicates that the resistance to the skidding of the wheels is more substantial on the LMS model than on the physical MHT. As will be seen in the results, this causes the robot to turn with more difficulty in simulation.

In simulation, the MHT remains stationary for 5 seconds to achieve the steering posture prior to the beginning of the leader-follower scenario. It should be noted that the posture reconfiguration maneuver causes the robot to rotate 3º in LMS Virtual.Lab Motion. The leader starts at 1 m in front of the MHT. Then, once the maneuver begins, the leader moves along a quarter-circular trajectory at constant linear velocity and turning rate of 0.2818 m/s and 5º/s. After 18 seconds into the maneuver, the leader stops and remains stationary until the end of the simulation. Fig. 7 illustrates the trajectories of the leader and of the MHT. Fig. 8 shows the performance of the leader-follower controller.

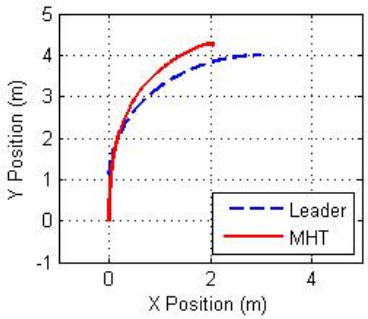

Figure 7: Leader-Follower Maneuver on Flat Terrain - Leader and MHT's Trajectories

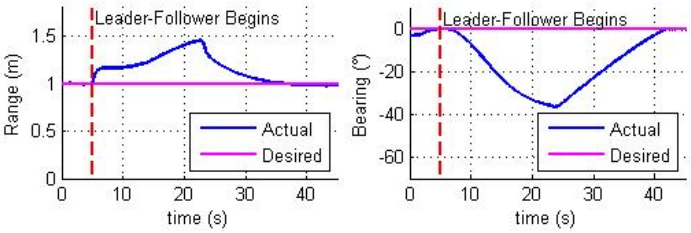

Figure 8: Leader-Follower Simulation on Flat Terrain – Leader-Follower Results

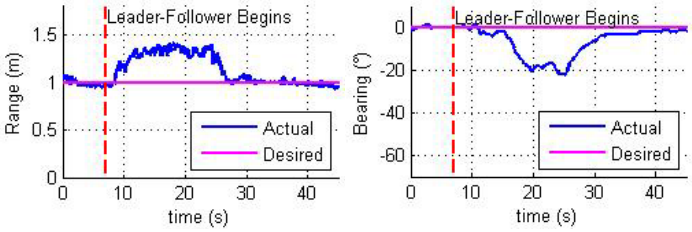

Figure 9: Leader-Follower Experiment on Flat Terrain - Leader-Follower Results

The same test was executed using the physical MHT prototype with, to the extent possible, the same conditions as in simulation. In the experiment, the robot remains stationary in the first 7 seconds maneuver to reconfigure its posture[1]. The leader is initially located 1 m in front of the MHT and is moved along the quarter-circular trajectory for 18 seconds, approximately as in simulation. Then, the leader stops and remains stationary until the end of the experiment. Fig. 9 illustrates the performance of the leader-follower controller with the physical robot.

Comparing Figs. 8 and 9, we observe similarities between the performance of the leader-follower controller in simulation and in the experiment. In both sets of results, the range and bearing errors increase as the leader-follower maneuver begins and remain high until the leader stops at 18 seconds into the maneuver. The range error stabilizes after 7 seconds during the experiment while it increases steadily during the simulation, peaking at 18 seconds. The maximum range error in the tests is 0.46 m in simulation and 0.42 m in the experiment, which are in good agreement. The maximum bearing error is 37º in simulation and 22º in the experiment. The bearing error stabilizes at 13 seconds into the leader-follower maneuver with the physical robot while it increases until the leader stops in simulation. Inspection of the turning rate of the MHT during the simulation revealed that the actual turning rate of the robot was significantly lower than the desired turning rate computed by the leader-follower controller. This is attributed to the high resistance to skidding of the wheels in the LMS model of the MHT, which affects the turning kinematics of the robot.

Once the leader stops, the range and bearing errors decrease rapidly in both the simulation and the experiment, reaching their desired values at 37 seconds into the maneuver in simulation and 28 seconds with the physical MHT. We remark that the robot does not reach the exact desired range and bearing in the experiment. This is due to the dead-zones added to the leader-follower controller implemented on the physical MHT. In summary, we observe that the physical MHT robot achieves better results than its LMS model. This is attributed to two factors: the gains of the leader-follower were not optimized for the LMS model of the MHT, and the high skidding resistance of the in simulation prevented the robot from reaching its desired turning rate. Nonetheless, in both tests, the leader-follower controller was able to navigate the MHT to achieve the desired leader-follower formation.

[1] The posture reconfiguration period was extended in the experiments to ensure that the MHT remained stable during the maneuver.

C. *Leader-Follower Maneuver on a Ramp*

To assess the MHT's ability to achieve leader-follower behavior and posture control simultaneously with the proposed controller, we implemented a leader-follower maneuver in which the robot is required to climb a 10º ramp to achieve leader-follower formation control. The ramp used in this scenario is 1.42 m long and ends with a flat platform (Fig. 10). The leader is positioned on top of the ramp at an initial range of 3.5 m in front of the MHT and does not move. The robot must achieve a desired range of 1 m from the leader. As the MHT negotiates the ramp, the posture controller is applied to maintain the posture of the robot at a zero pitch and roll angles, and a chassis height of 0.409 m. To prevent the MHT from losing its stability during the maneuver, we increased the wheel separation of the robot to 0.930 m. As well, because the ramp employed in the maneuver is not much wider than the MHT, we overrode the turning rate computed by the leader-follower controller to be zero in order to prevent the robot from moving off the ramp. Thus, the MHT is not expected to regulate its bearing. However, the bearing plot is included for completeness.

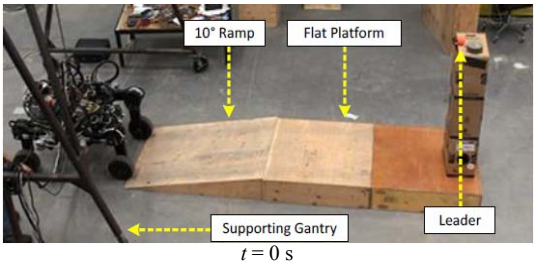

$t = 0$ s

$t = 7$ s

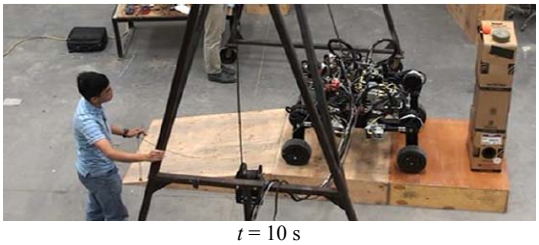

$t = 10$ s

Figure 10: Leader-Follower Maneuver on Ramp - Snapshots

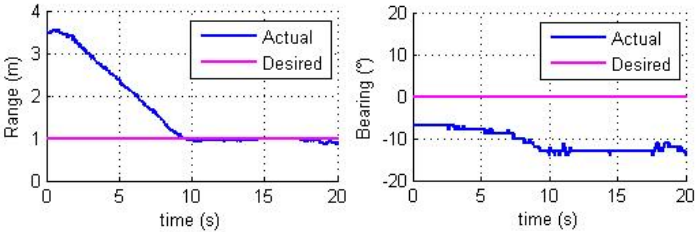

Figure 11: Leader-Follower Maneuver on Ramp - Leader-Follower Results

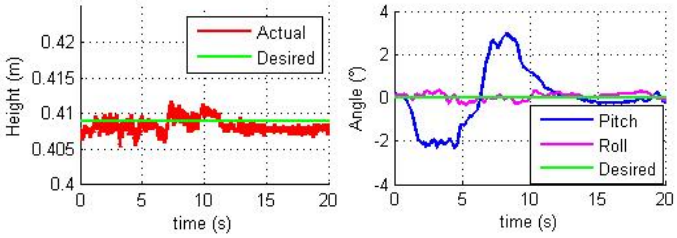

Figure 12: Leader-Follower Maneuver on Ramp - Posture Controller Results

This maneuver was executed on the physical MHT prototype. Fig. 10 shows snapshots of the MHT during the experiment. The performance of the leader-follower controller during the maneuver is presented in Fig. 11. Fig. 12 illustrates the results of the posture controller of the MHT. As seen in the plots, the MHT achieves the desired range after 9 seconds into the maneuver. We observe that the robot does not reach the desired bearing, which was anticipated since the steering command of the leader-follower controller was disabled for this test. As the MHT negotiates the ramp, the posture controller readjusts the height of each leg to correct the pitch angle error of the chassis while maintaining the desired chassis height (Fig. 10). In Fig. 12, we can observe that the posture controller maintains the posture parameters of the MHT close to their desired values as the robot moves up the ramp. The roll angle remains zero during the maneuver and the chassis height has a steady state error of 0.004 m. The maximum pitch angle error is 3º. The deviations in the pitch angle of the MHT occur when the robot starts to negotiate the ramp and when it reaches the end of the ramp. In summary, the leader-follower maneuver on ramp demonstrates that the controller presented in this paper is capable of operating the MHT to achieve leader-follower formation control and posture control simultaneously.

V. Conclusion

In this paper, we have presented a leader-follower controller for the MHT, a skid-steering wheel-legged vehicle. The controller uses the range and bearing of a designated leader to compute the desired wheel velocities of the MHT to achieve leader-follower formation control. We implemented the leader-follower controller in parallel with a velocity-based inverse kinematics controller developed in previous work to allow the robot to achieve leader-follower behavior and posture control *simultaneously*. The proposed controller was validated in simulation and with the physical MHT prototype. The robot uses a vision system to track the position of the leader. Comparison between the simulated and experimental results showed reasonable qualitative agreement in the range and bearing responses of the controller. The differences in the results were attributed to the higher skidding resistance of the wheels in the simulation of the MHT, which is one aspect to resolve in future work. We also demonstrated the combined execution of leader-follower formation control and posture control of the vehicle on a ramped surface, which illustrates the MHT's ability to regulate its posture while tracking a leader on uneven terrain.

Acknowledgment

This work was supported with funding from Defence Research and Development Canada, the Natural Sciences and Engineering Research Council of Canada, McGill University and Hydro-Quebec. The simulations and experiments on the MHT were made possible with the collaboration of DRDC – Suffield Research Centre.

References

[1] W. Burgard, M. Moors, D. Fox, R. Simmons, and S. Thrun, "Collaborative multi-robot exploration," in *IEEE International Conference on Robotics and Automation*, 2000, pp. 476-481.

[2] D. Quoc Khanh and S. Young-Soo, "Human-following robot using infrared camera," in *IEEE International Conference on Control, Automation and Systems*, 2011, pp. 1054-1058.

[3] G. W. Gamage, G. K. Mann, and R. G. Gosine, "Leader follower based formation control strategies for nonholonomic mobile robots: design, implementation and experimental validation," in *American Control Conference*, 2010, pp. 224-229.

[4] J. Ghommam, H. Mehrjerdi, and M. Saad, "Leader-follower based formation control of nonholonomic robots using the virtual vehicle approach," in *IEEE International Conference on Mechatronics*, 2011, pp. 516-521.

[5] L. Consolini, F. Morbidi, D. Prattichizzo, and M. Tosques, "Leader–follower formation control of nonholonomic mobile robots with input constraints," *Automatica,* vol. 44, pp. 1343-1349, 2008.

[6] I.-S. Choi and J.-S. Choi, "Leader-follower formation control using PID controller," in *Intelligent Robotics and Applications*. vol. 7507, C.-Y. Su, S. Rakheja, and H. Liu, Eds., ed: Springer Berlin Heidelberg, 2012, pp. 625-634.

[7] K. Iagnemma and S. Dubowsky, *Mobile robots in rough terrain : estimation, motion planning, and control with application to planetary rovers*. Berlin: Springer Berlin Heidelberg, 2004.

[8] T. Thomson, I. Sharf, and B. Beckman, "Kinematic control and posture optimization of a redundantly actuated quadruped robot," in *IEEE International Conference on Robotics and Automation*, 2012, pp. 1895-1900.

[9] C. Grand, F. BenAmar, F. Plumet, and P. Bidaud, "Decoupled control of posture and trajectory of the hybrid wheel-legged robot hylos," in *IEEE International Conference on Robotics and Automation*, 2004, pp. 5111-5116.

[10] B. Beckman, J. Pieper, D. Mackay, M. Trentini, and D. Erickson, "Two dimensional dynamic stability for reconfigurable robots designed to traverse rough terrain," in *IEEE/RSJ International Conference on Intelligent Robots and Systems*, 2008, pp. 2447-2452.

[11] C. Wong, "Posture reconfiguration and step climbing maneuvers for a wheel-legged robot," Master Thesis, Department of Mechanical Engineering, McGill University, Montreal, 2014.

[12] B. Bona and M. Indri, "Friction Compensation in Robotics: an Overview," in *44th IEEE Conference on Decision and Control and European Control Conference*, 2005, pp. 4360-4367.

[13] T. Thomson, "Kinematic control and posture optimization of a redundantly actuated quadruped robot," Master Thesis, Department of Mechanical Engineering, McGill University, Montreal, 2011.

[14] G. R. Bradski, "Real time face and object tracking as a component of a perceptual user interface," in *4th IEEE Workshop on Applications of Computer Vision*, 1998, pp. 214-219.

[15] Itseez. (2014). *OpenCV Website*. Available: http://opencv.org/